Broadband Full Field of View Imaging with Computational Mirrors

Vishwanath Saragadam[1], Niki Nezakati[1], Amit Roy-Chowdhury[1], and Vivek Boominathan[2]

[1] University of California Riverside, Riverside CA 92521, USA
[2] Rice University, Houston, TX 77005, USA
vishwanath.saragadam@ucr.edu
https://codelab-ucr.github.io/computational-mirrors/

Abstract. Traditional glass-based optics are typically optimized for narrow spectral bands, such as the visible (400–700nm) or shortwave infrared (1000–1800nm). While the emergence of VIS-SWIR sensors (400–1700nm) offers transformative potential, refractive optics struggle to focus this entire range simultaneously. Mirrors represent a promising achromatic alternative; however, they are often sidelined by field curvature, and off-axis aberrations. This paper introduces **Computational Mirrors**, a framework that enables high-resolution, full-field-of-view imaging across the complete VIS-SWIR spectrum using a single sensor. Our method is built on the observation that distinct regions of the field of view reach focus at varying distances from the mirror. By capturing a minimal focal stack (2–4 images), we utilize a computational backend to recover a sharp, all-in-focus image. A key contribution of this paper is **Seidel-Conv**, a novel, physics-inspired, spatially-varying point spread function (PSF) model designed to accurately characterize and correct the off-axis aberrations inherent in simple concave mirrors. We demonstrate the efficacy of our approach using a first-of-its-kind 50mm F/1 optical system equipped with a VIS-SWIR sensor. Our system produces sharp images across RGB, NIR, and SWIR wavelengths without requiring refocusing, revealing material details invisible within individual spectral bands. We further validate the scalability of our approach with a 100mm F/2 system optimized for long-range imaging.

1 Introduction

Recent advancements in sensor technology have unlocked imaging capabilities across an expansive spectral range, spanning from the visible to the short-wave infrared (SWIR) wavelengths. These broadband sensors enable high-accuracy material classification [1–3], robust imaging in extreme weather conditions due to low scattering in SWIR [4], and increased visibility in the dark [5]. However, the optics required to focus such broadband light remain a bottleneck. Traditional refractive (glass-based) optics are inherently limited by chromatic aberration, where different wavelengths focus at different depths due to the dispersive nature of glass (Fig. 1(a)). To mitigate this, optical designers rely on complex,

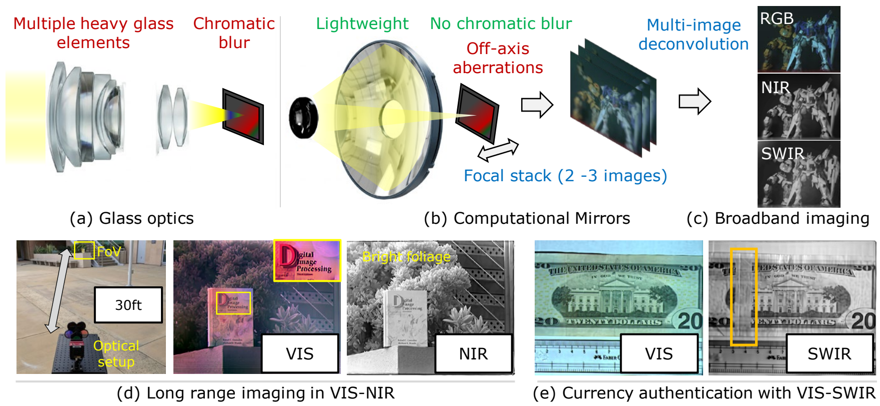

Fig. 1: Computational mirrors. (a) Traditional refractive (glass) optics require complex, multi-element assemblies that are inherently bulky and prone to chromatic aberration across the VIS-SWIR spectrum. In contrast, reflective optics are achromatic but suffer from severe off-axis geometric aberrations. (b) Our approach captures a sparse focal stack using simple mirror optics and employs a multi-image deconvolution backend to recover a sharp, full-field-of-view image. (c) The proposed system enables high-performance, ultra-broadband imaging (400–1700nm) using a compact hardware footprint. (d) Long-Range Imaging: Demonstration of sharp, multi-spectral capture at significant distances across visible and NIR bands. (e) Material Analysis: An application in currency authentication, where imaging across visible and SWIR wavelengths reveals security features invisible to standard sensors.

heavy, and often prohibitively expensive multi-element assemblies to align the broad spectral range onto a single focal plane. This complexity frequently leads to undesirable trade-offs, such as restricting the system to a narrow subset of wavelengths or bulky multi-camera architectures to cover the full spectrum.

Reflective optics, including concave mirrors and complex multi-mirror objectives [6], are inherently achromatic from the deep UV to the far-infrared. This characteristic makes them theoretically ideal for VIS-SWIR imaging. Consequently, reflective designs are standard in specialized fields such as microscopy [7] and large-scale astronomical instrumentation, most notably the James Webb Space Telescope (JWST) [8]. However, mirrors, particularly simple configurations with only one or two focusing elements, suffer from severe off-axis aberrations that constrain their versatility. These distortions typically limit the usable field of view (often to 1mm or less in microscope objectives) or necessitate high f-numbers ($f/6$ or higher), which significantly reduces light throughput. One particularly debilitating effect in few-mirror systems is the Petzval (field) curvature [9]. In these systems, the image surface is non-planar; different regions across the field of view reach focus at varying distances from the mirror. This characteristic renders traditional mirror-based solutions impractical for medium focal lengths (50–100mm), where a flat sensor cannot simultaneously capture a sharp image across the entire frame.

This paper presents **Computational Mirrors**, a practical imaging pipeline that combines hardware-controlled focal stack acquisition with a physically motivated forward model and multi-image reconstruction. Our approach is based on two primary contributions: First, we demonstrate that while a single exposure from a simple mirror optic suffers from severe field curvature, a focal stack effectively captures sharp regions of the scene at varying axial positions. By capturing a minimal stack (2–4 images), we ensure that every point in the full field of view is sampled at or near its focus (Fig. 1(b)). We then employ multi-image deconvolution to fuse these measurements into a single, high-fidelity, all-in-focus image. However, these raw focal stack images are still degraded by complex off-axis aberrations. Traditional restoration methods, such as patch-wise convolution or Eigen-decomposed PSF models, are insufficient for modeling these spatial variations inherent in high-aperture mirror systems. To address this, we propose **SeidelConv**, a novel physics-inspired PSF model. Drawing inspiration from Spatial Transformer Networks [10], SeidelConv accurately characterizes the spatially-varying blur across each image in the stack. SeidelConv is built on the observation that off-axis aberrations can be effectively modeled as localized geometric distortions. The input image is warped by a small set of affine transformations (typically 20 - 30) that models the distortions inherent to off-axis aberrations. These images are then blurred by learned kernels, and then weighed by per-pixel weights and summed. These parameters, including the affine matrices, blur kernels, and weight maps, are optimized using a monitor-based calibration procedure [11]. Finally, we integrate the SeidelConv forward model into a Plug-and-Play (PnP) framework [12] to recover the final sharp image, leveraging deep priors for robust regularization (Fig. 1(c)).

We validate the efficacy of Computational Mirrors through experimental prototypes using $f/1$ 50mm and $f/2$ 100mm concave mirror objectives. These are paired with a Sony IMX990 VIS-SWIR sensor, capable of sensing from 400nm to 1700nm. Computational mirrors generalizes beyond controlled lab settings to real world scenes at arbitrary depths. Across a diverse array of real-world scenes, ranging from macro-scale material analysis of currency to long-range outdoor environments, our system captures high-fidelity imagery across the Visible (400–700nm), NIR (700–1000nm), and SWIR (1000–1700nm) bands (Fig. 1(d,e)). Our approach eliminates the need for wavelength-dependent refocusing, a common failure point in refractive broadband systems. These results represent the first demonstration of high-aperture ($f/1$), ultra-broadband imaging using simple reflective optics. By overcoming the traditional limits of field curvature and off-axis aberrations, this work paves the way for a new compact, lightweight, and cost-effective solutions for multi- and hyperspectral imaging.

2 Prior Work

Our work builds on results in aberration theory of curved surfaces such as mirrors and lenses, focal stacking and computational imaging, and broadband imaging. We explore the prior work in these areas next.

Optical aberrations. Optical aberrations are broadly categorized under geometric and chromatic aberrations. Geometric aberrations occur due to light rays of a single wavelength not focusing at a single point either on axis or off-axis. These aberrations are categorized by Seidel aberrations [13]. Additionally, these optics may suffer from the Petzval field curvature, where the focused surface is not planar but a curved one. These aberrations are common to both glass and mirror optics, and are often corrected with multi element design [14]. Chromatic aberrations occur when light of various wavelengths do not focus at the same point, resulting in longitudinal (focal shift), and sometimes off-axis aberrations. This is inherent to glass-based optics, and is corrected by using glass optics with various refractive index to cancel out the aberrations. Invariably, while glass-based optics can produce very large field of view images, they are limited to a narrow range of wavelengths.

Diffractive and metasurface optics. Diffractive optical elements (DOEs) and meta-optics offer a flat-optic alternative to conventional imaging [15,16]. Similar to DOEs, Mao et al. [17] use a deformable phase plate to locally correct aberrations across the field and stacking the results into a sharp composite. However, these designs remain limited to the visible band and apertures on the order of 1 cm or smaller, which is considerably below the 50–100 mm, broadband VIS–SWIR objectives we target. Hybrid optics that consist of glass elements and DOEs are a promising alternative [18–20] that combines complementary dispersion due to glass and DOEs. However, hybrid optics are challenging to design, and sensitive to element placement. Mirrors have no chromatic aberrations, and are compact, but suffer from off-axis aberrations and field curvature (see Fig. 2).

Mirror-based imaging optics. Mirror-based objectives are the workhorse of astronomy, where broadband focusing, high light throughput, and light weight are critical. To this end, most observatories, and space telescopes (Hubble, Roman, JWST) are equipped with mirror-based optics, often with 3 or more elements in a so-called anastigmat configuration to obtain diffraction limited performance across the whole field of view. However, these telescopes are often operated at f/10–f/20 and thus have very long focal lengths to image at high spatial resolution. In the microscopic world, commercial off-the-shelf reflective objectives enable achromatic imaging from 400nm to 20μm. These objectives are in the Schwarzchild configuration [7] which consists of a concave and a convex mirror with the same curvature to achieve sharp images over the field of view. However, these objectives have extremely narrow field of view due to strong Petzval field curvature. These limitations often lead to catadioptric [21] solutions where mirrors are combined with lenses to get large field of view [22]. However, the presence of a lens causes chromatic aberrations, invariably leading to blurry results. It is possible to build curved sensors that approximately follow the Petzval curvature of mirrors, but only works for a fixed mirror objective. To this end, for imaging macro world, and for hyperspectral objectives, there are no known purely mirror-based objectives between 50-100mm with large light collection capabilities that work with flat sensors.

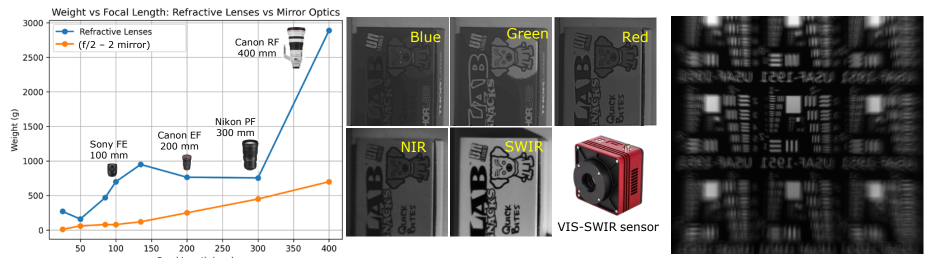

(a) Size and weight advantages of mirrors (b) Full broadband imaging capability (c) Strong off-axis aberrations

Method	Compact and light weight	Broadband imaging	Full FoV imaging
Refractive optics	×	×	✓
Reflective optics	✓	✓	×
Computational Mirrors + SeidelConv (proposed)	✓	✓	✓

Fig. 2: Challenges and opportunities with mirrors. Mirrors have two unique advantages. (a) they are considerably lighter in weight and size compared to refractive optics, and (b) they can focus light across extremely broadband wavelengths. When equipped with VIS-SWIR sensors, they can enable broadband imaging with no wavelength-dependent corrections. However (c) mirrors suffer from strong off-axis aberrations where only the center is in focus. We present a computational approach to obtain sharp images from such aberrated images using mirror-based optics.

Computational corrections for imaging with mirrors. Yokoya and Nayar [23] demonstrated that a focal stack of images, when summed up, enabled spatially invariant blur, which can then be input to a deconvolution algorithm. In lens-based optics, Matsunaga and Nayar [24] showed that a dense focal stack can be leveraged to evaluate an image on the Petzval curved surface, and then can be deconvolved with a spatially invariant blur. Other work achieves snapshot multi-focus capture through beam splitters or specialized optics [25], trading light efficiency for acquisition speed. Most prior works have relied on dense focal stacks (10 - 30 images) to enable a sharp image, which is often impractical in real settings. We build on these ideas but tailor our method to the structure of mirror-based imaging. Rather than collapsing to a single image (by summing or evaluating on the Petzval surface), we perform a multi-image deconvolution with the focal stack. In such conditions, we show that as few as 3 images suffice to obtain a very sharp image, even with F/1 optics, enabling high throughput, broadband imaging capabilities.

3 Computational Mirrors

We now detail the hardware and algorithm used for overcoming the physical limitations of single element mirror-based objectives.

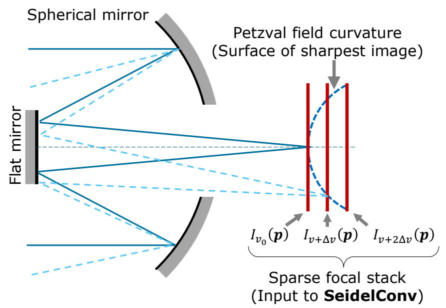

(**a**) Imaging with mirror optics showing Petzval curvature and our sparse focal stack measurement

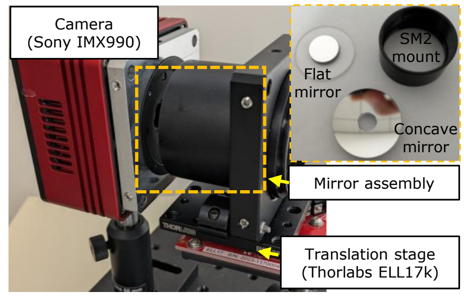

(**b**) Our optical setup with broadband (400-1700nm) image sensor and mirror objective

Fig. 3: Computational mirrors hardware. (a) Mirror optics enable imaging without any chromatic aberration but suffer from severe field curvature. To tackle this, we leverage a computational reconstruction approach by measuring a sparse focal stack that spans the whole Petzval curved field, and then perform a multi-image deconvolution with our proposed SeidelConv. (b) shows our optical setup with a broadband VIS-SWIR sensor (ToupTek SensWIR 1.3MP), a translation stage to capture the focal stack, our constructed mirror objective, and five spectral filters spanning blue, green, red, NIR, and SWIR to demonstrate broadband imaging capabilities.

3.1 Construction of Mirror Objective

Our objective is engineered to mimic the form factor and optical alignment of traditional refractive lenses, ensuring seamless integration as a drop-in replacement within standard imaging architectures (Fig. 3). The assembly utilizes a primary concave mirror that focuses light through a central aperture. A secondary planar fold mirror is positioned to redirect the optical path, significantly reducing the system's longitudinal footprint and simplifying mechanical alignment. In our prototype, the fold mirror is secured to a planar glass substrate, providing a stable reference for precise, repeatable capture. The sensor is interfaced with a motorized linear translation stage aligned with the optical axis. By translating the sensor, we acquire a focal stack that samples the non-planar image surface. This axial sweep is a fundamental requirement of the system; because simple reflective objectives exhibit pronounced Petzval curvature, on-axis and off-axis regions reach their respective focal planes at different depths. Capturing the full focal stack ensures that every point across the full field of view is sampled at its optimal focus. All data is recorded using a Sony IMX990 VIS-SWIR sensor, enabling broadband intensity measurements across the 400–1700nm spectrum.

3.2 Focus Stacking

Due to Petzval curvature, a simple mirror objective cannot form a sharp image across the entire field of view (FoV) on a flat sensor (see Fig. 3(a)). One straightforward approach is to capture a dense focal stack that fully samples the volume containing the curved image surface, a technique previously explored by Matsunaga et al. [24]. This approach is often impractical for real-world deployment, as it typically requires 30 or more exposures to adequately cover the Petzval surface. Furthermore, Matsunaga et al. relied on spatially invariant deconvolution to address residual blur. This remains insufficient for high-aperture reflective systems, where the sharpest points on the Petzval surface still suffer from significant spatially varying aberrations, such as coma and astigmatism, that necessitate a more sophisticated, non-uniform PSF model.

Sparse focal stack capture. We instead capture a sparse focal stack consisting of only N images (typically 2-4), to span the depth of the Petzval curvature. We demonstrate that performing joint multi-image deconvolution on this sparse set yields image quality comparable to, or exceeding, that of a dense stack while significantly reducing acquisition time and data overhead.

By mounting the mirror objective on a motorized translation stage, we can sample the focal volume at arbitrary axial positions. We first move the translation stage that enables the sharpest view in the center of the FoV. Let this position be $v = v_0$, and let the corresponding image be $I_{v_0}(\mathbf{p}) \in \mathbb{R}^{H \times W}$, where H and W are number of rows and columns in the image respectively and $\mathbf{p}$ is the 2D coordinate in the image. We then capture a total of N images, each separated by a constant axial step Δv. The images in the focal stack are hence, $\{I_{v_0+k\Delta v}(\mathbf{p})\}_{k=0}^{N-1}$. N typically depends on the curvature of the field. In practice, we found that $N = 3$ is sufficient to ensure that every point $\mathbf{p}$ in the FoV is sampled near its optimal focus in at least one measurement. Consequently, at each spatial coordinate, the stack provides N distinct measurements of the scene, allowing us to treat the recovery of a single sharp image, $I_0(\mathbf{p})$, as a well-posed multi-image inverse problem. To solve this, we first define a computationally tractable forward operator capable of modeling the severe, spatially varying off-axis aberrations across the stack.

3.3 SeidelConv: Physics-inspired PSF modeling

The off-axis aberrations at each focal stack position stem from astigmatism, coma, and often spherical aberrations, which are often modeled as Seidel aberrations [13]. Approaches such as patch-wise PSF modeling [26] or Eigen decomposition of PSF [27] are ill suited to model such extreme off-axis aberrations spanning several tens of pixels. While microscopic or ideal systems are often modeled with radial or circular symmetry [28–30], real-world reflective assemblies frequently suffer from mechanical misalignment during mounting. In our experiments, we found that PSF models based on radial symmetry [29] perform poorly in off-axis regions in practical systems. This observation necessitates a flexible, learned model that can characterize arbitrary, non-symmetric PSF variations across the sensor.

Inspired by the classical Seidel aberrations [13] of optical systems that depend on pupil and image-space coordinates, and recent works in atmospheric turbulence modeling [31], we propose a novel spatially varying PSF model designed to characterize the severe aberrations inherent in reflective optics. We formulate each measurement in the focal stack as:

$$I^{(k)}(\mathbf{p}) = I_{v_0+k\Delta v}(\mathbf{p}) = \mathcal{A}^{(k)}(I_0(\mathbf{p})) + \eta^{(k)}, \tag{1}$$

where $\eta^{(k)}$ accounts for noise and model mismatch, and $\mathcal{A}^{(k)}$ is a spatially varying blur operator. Our operator, SeidelConv, parametrizes the local PSF as a mixture of a small set of basis kernels with spatially varying weights and bounded affine deformation. The bounded affine transforms are similar in spirit to the Seidel aberrations that are expressed as function of spatial (polar) coordinates. However, SeidelConv is sufficiently flexible to account for practical systems where the optics are potentially misaligned. The SeidelConv forward operator for the k^{th} image is,

$$I^{(k)}(\mathbf{p}) = \sum_{q=1}^{Q} \underbrace{w_q^{(k)}(\mathbf{p})}_{\text{per-pixel weight}} \underbrace{I_0(\phi_q^{(k)}(\mathbf{p}))}_{\text{warping}} * \underbrace{h_q^{(k)}(\mathbf{p})}_{\text{blurring}}, \tag{2}$$

where $w_q^{(k)}$ is the per-pixel weight, $\phi_q^{(k)}$ is a coordinate warping operator (in our case, an affine function), and $h_q^{(k)}(\mathbf{p})$ is the blur kernel, all for the k^{th} image (See Fig. 4 (a)). We model the warping operator as an affine function,

$$\phi_q^{(k)}(\mathbf{p}) = R_q^{(k)}\mathbf{p} + \mathbf{t}_q^{(k)}. \tag{3}$$

Note that in the absence of affine warping, SeidelConv is similar to CoordGate [32] or a learning variant of EigenCWD [27]. However, the inclusion of the warping operation provides a critical geometric degree of freedom, allowing the model to precisely characterize the stretching and rotation of PSFs (e.g., coma and astigmatism) as they move off-axis. As demonstrated in our results, this makes SeidelConv considerably more effective at modeling the extreme aberrations typical of high-aperture mirror optics.

Multi-Image Deconvolution. Assuming the parameters of the PSF model are learned, we solve a multi image problem to estimate the latent sharp image $I_0(\mathbf{p})$ by solving a simple optimization problem,

$$\min_{I_0(\mathbf{p})} \sum_{k=1}^{N} \left\| \mathcal{A}^{(k)}(I_0(\mathbf{p})) - I^{(k)}(\mathbf{p}) \right\|_2^2 + \lambda\, \mathcal{R}(I_0(\mathbf{p})), \tag{4}$$

where $\mathcal{R}(\cdot)$ is an image prior, which could be a simple total variational loss, a deep image prior, or, as in our case, a plug-and-play denoiser. This multi-image deconvolution enables considerably higher quality results compared to converting a focal stack into a single sharp image, or averaging the focal stack into a single blurred image with spatially invariant kernel (See Fig. 4(b)).

SeidelConv calibration. To calibrate the parameters θ_k (affine matrices, blur kernels, and per-pixel weights) of $A^{(k)}$, we leverage a monitor-based calibration approach [11]. Specifically, we display a random set of dots on a monitor placed

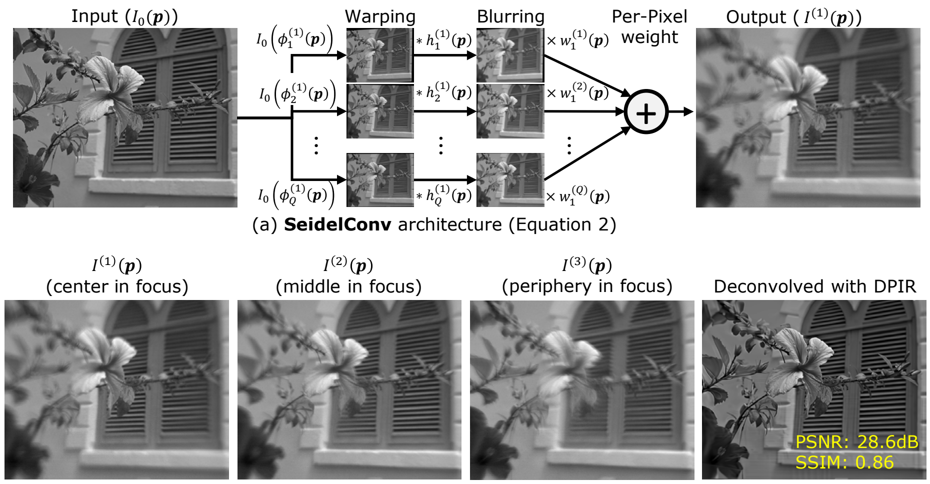

(b) Deconvolution Pipeline (Equation 4)

Fig. 4: SeidelConv architecture. (a) shows SeidelConv architecture described in eq. (2) for learning the forward operator for a single wavelength range. The input image is warped by an affine (inspired by Seidel aberrations), and each warped image is blurred and weighed in a per-pixel manner and summed to get the output. (b) shows three images captured with our optical setup for the green wavelengths, and the deconvolved result by combining SeidelConv with a plug-and-play prior [12], described in eq. (4). Each of the three focus settings captures a near sharp image in various regions. Our multi-focal deconvolution algorithm generates a single sharp image that is focused over the full FoV.

a fixed distance away from the optical setup. Then, we measure focal stack with relevant v_0 such that the center is in focus, along with a total of N images placed Δv apart (See Fig. 5). We then solve a stochastic gradient descent problem with the following optimization function,

$$\min_{\{\theta_k\}_{k=0}^{N-1}} \sum_{l=1}^{L} \sum_{k=1}^{N} \left\| \mathcal{A}_{\theta_k}^{(k)}(I_0^i(\mathbf{p})) - I^{(k),i} \right\|_2^2 + \lambda_{\text{kern}} \sum_{k=1}^{K} \|h_k\|_1, \tag{5}$$

for L calibration images. We regularize the blur kernels by imposing a ℓ_1 norm to ensure sparsity. In our experiments, we used $L = 10$ images for training the parameters, for $N = 3$ focal stack images. Further details about calibration, including offset and vignetting calibration are available in the supplementary. Post calibration, the sensor can be at any arbitrary v_0 as long as the center part of the image is in focus. However, the spacing between focal stack images, Δv is to be fixed. Fig. 5 shows the measurements for 50mm F/1 mirror at three focus settings and the output of the learned SeidelConv operator.

Generalization of PSF model to arbitrary wavelength range. A unique advantage of mirror-based optics is that the PSF is nearly invariant to wavelength. This

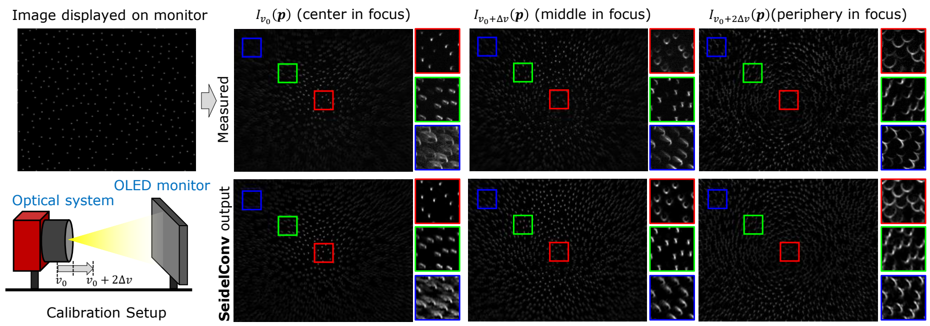

Fig. 5: Accuracy of PSF calibration. The first column shows the calibration setup, where we displayed an image with sparse and random dots on an OLED monitor. The next three columns shows a random set of dots for three focus settings, (top row) measured by the optical system and (bottom row) output by SeidelConv. The model accurate captures the highly varying PSF with an error of 4×10^{-3}, enabling accurate deconvolution across the full field of view.

implies SeidelConv can be calibrated over any range of wavelengths and applied to any other range of wavelengths. We calibrated SeidelConv using broadband visible light (400–700nm) and successfully deconvolved images across the entire VIS-SWIR spectrum (400–1800nm) without fine-tuning. This flexible capability is impractical with glass optics, where material dispersion necessitates unique focus settings or separate PSF models for each spectral band. Our approach bypasses these bottlenecks, enabling seamless cross-spectral imaging with a single hardware calibration.

Sensitivity to Object distance. The PSF of imaging systems is mildly sensitive to object position. For mirrors, the field curvature, is independent of object distance, implying that our approach of focal stack with fixed inter-image distance scans the same Petzval curvature. Further, we empirically observed that the PSF does not significantly change for most practical object distances. Specifically, we observed that the PSF at calibration distance and beyond that distance had a 2D autocorrelation of 0.94, emphasizing that it was sufficient to calibrate the PSF model at one single plane.

4 Results

We now show experimental validation of our system using the prototype shown in Fig. 3. All the results in this section are real captures. Panchromatic (grayscale) images were captured without any optical filter. For multispectral experiments, we utilized a filter wheel equipped with 2-inch spectral filters, including Blue, Green, Red, NIR, and SWIR, positioned in front of the objective. The initial axial position of the objective, u_0, was optimized per-scene to ensure the center of the field of view (FoV) was at peak focus. The translation step size, Δu, was held constant at 200 μm for all experiments with 50mm objective, and 100μm for all experiments with 100mm objective. Our 50mm objective achieves a full field of view of 18° with the VISSWIR image sensor, while the 100mm objective achieves 9°. For the SeidelConv architecture, we utilized a mixture of $Q = 31$ basis components, each consisting of an affine transformation and an 11×11 blur kernel. The model was implemented in PyTorch and trained on a calibration set of 10 images using a learning rate of 5×10^{-3}. For the reconstruction phase, we employed the grayscale version of DPIR [12] as our plug-and-play prior. Notably, the same model was applied across all five spectral bands individually without any per-band fine-tuning, demonstrating the robust achromaticity of our reflective design. Additional details are available in the supplement.

Deconvolution performance. Fig. 4 shows three captured images, and the resultant deconvolved image with SeidelConv. The three images exhibit sharpness in various regions of the FoV, as a result of Petzval curvature. Effectively, the focal stack images are intersecting the Petzval surface at various points. SeidelConv is able to recover a sharp image across the full field of view. Additional evaluations on the effect of parameters are in the supplement.

Comparison against other PSF models. To evaluate the efficacy of SeidelConv, we compared its performance against several state-of-the-art PSF models while maintaining identical deconvolution parameters across all tests. We curated a validation dataset by displaying 20 images from the Kodak dataset [34] on a radiometrically calibrated OLED display. To ensure strict radiometric accuracy, we utilized only the green channel. Performance was quantified using Peak Signal-to-Noise-Ratio (PSNR) and Structural Similarity Index (SSIM). As shown in the USAF test target comparison (Fig. 6, top row), the importance of coordinate warping is clear. CoordGate model fails to compensate for extreme off-axis aberrations. While patch-wise convolution with a 21×21 kernel provided the second-best results, it remained qualitatively inferior to SeidelConv. The table in Fig. 6 shows metrics for the baselines including various PSF models for multi-image deconvolution with three images, deconvolution by summing up the focal stack [23], deconvolution of the Petzval curvature image [24], and a single image deconvolution with one image in the focal stack [33] with various PSF models including ours, and Ring Deconvolution [29]. We evaluated both on-axis metrics (center half) and off-axis metrics (everything other than center half). While on-axis performance is comparable across most methods, SeidelConv significantly outperforms all baselines (more than 2dB higher) on off-axis. This highlights that affine warping is the key enabling factor for correcting the severe geometric distortions in full-field reflective optics.

Multispectral imaging results with 50mm objective. Fig. 7 (top rows) shows various scenes captured in the lab with our optical setup. Row 1 shows an opaque bag with a robot inside that is only visible in SWIR image. Row 2 shows a bottle of liquid that is once again only visible in SWIR. Row 3 shows a book and a plush toy. The plush toy loses all color in SWIR. Finally, row 4 shows

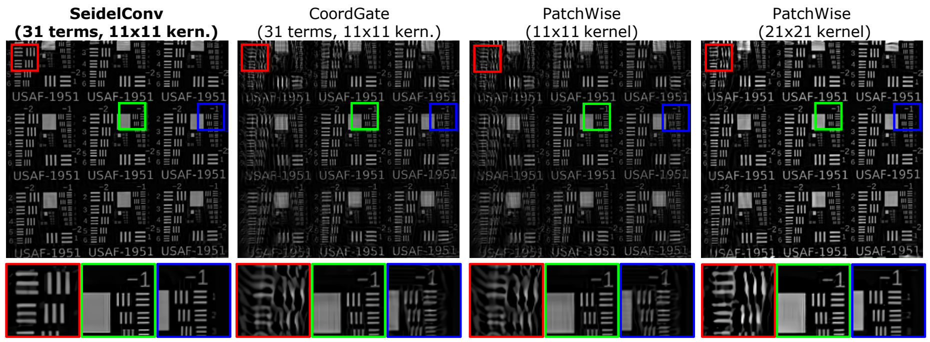

# Focal stack images	PSF model	Metrics On-Axis (P/S)	Metrics Off-Axis (P/S)
3 (**Computational mirrors**)	**SeidelConv** (11×11 kern.)	27.6/**0.84**	**27.1**/**0.74**
	CoordGate	27.6/0.80	24.8/0.63
	Patch-wise (11×11 kern.)	27.6/0.80	24.8/0.63
	Patch-wise (21×21 kern.)	**27.9**/0.80	21.6/0.65
20 → 1 [23] (Focal stack average)	**SeidelConv**	27.3/0.74	23.1/0.64
20 → 1 [24] (Image on Petzval surface)	**SeidelConv**	27.6/0.80	23.9/0.67
1 [33]	**SeidelConv**	25.6/0.66	20.9/0.49
	Ring Deconvolution [29]	22.7/0.52	18.7/0.29

Fig. 6: Comparison against other PSF models. The figure above shows deconvolution results with various PSF models including SeidelConv, CoordGate [32] that does not include warping, and two variants of patch-wise convolution with two kernel sizes. The table reports PSNR and SSIM evaluated on-axis (green box) and off-axis (red and blue box). All baselines perform similarly on axis, where the PSFs are compact. However, for off-axis, SeidelConv outperforms other models, demonstrating its importance for computational mirrors. The next three rows compare prior hardware-based approaches with SeidelConv PSF model. We observe that a multi-image deconvolution outperforms single-image, focal stack sum, or imaging on the Petzval surface.

two colorful robots with rich spatial texture. Across the board, our 50mm F/1 objective enables sharp images from 400nm all the way to 1700nm with a single focal setting. SeidelConv ensures that the resultant images are sharp across the whole field of view. The advantages of such an optic are evident in the rich and diverse set of features captured in individual wavelengths.

Long focal length imaging. Fig. 7 (bottom rows) shows results with 100mm F/2 optics with other configurations similar to the 50mm optic. A separate set of forward operators were learned for the 100mm optic. Objects were placed 6-10 feet away to demonstrate material identification. First row shows a genuine \$20 note, where the SWIR image shows a blank band to differentiate it from counterfeit notes. Second row shows a real (foreground) and artificial plant, that

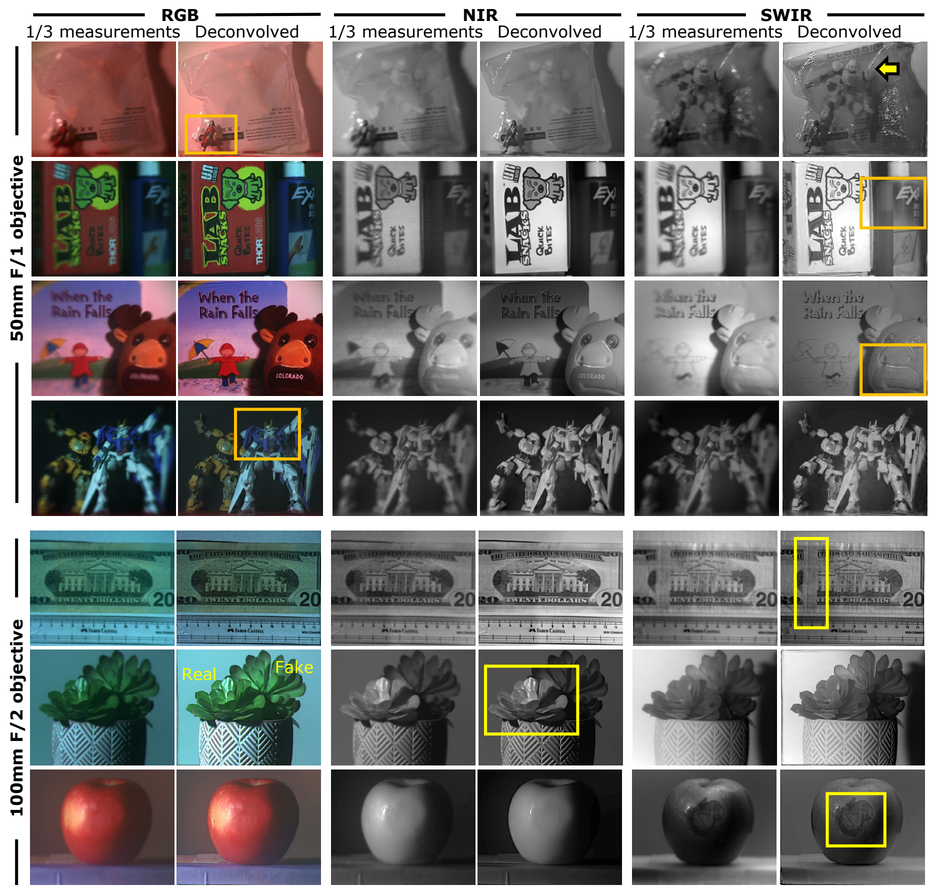

Fig. 7: High-resolution VIS-SWIR multispectral imaging. The figure above shows raw images and reconstructions with the mirror optic in RGB, NIR, and SWIR wavelengths for 50mm F/1 objective, and 100mm F/2 objective. Data was captured with the same focus settings, and five different spectral filters (red, green, blue, NIR, SWIR). Individual images were then deconvolved with 3-image focal stack. Each set of wavelengths captures complementary information. RGB captures texture, NIR captures material and foliate information (real vs. fake plant), and SWIR is excellent for imaging through thin occluders (plastic bags and bottles) and for forensics (20 dollar note). Our computational correction enables sharp images independent of choice of wavelength with only three images per wavelength, requiring no brittle wavelength-specific calibration, or wavelength-specific refocusing.

look nearly the same in RGB and SWIR wavelengths, but the real plant looks considerably brighter in NIR wavelengths. Third row shows an apple with a bruise, which is not visible in RGB or NIR, but distinctly visible in SWIR. Though the blur is less severe than 50mm objective, it nevertheless results in

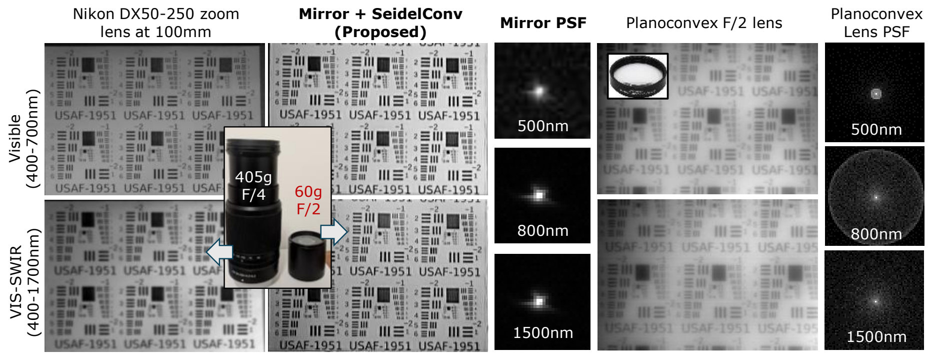

Fig. 8: Advantages of Mirrors. We compare visible and broadband (400 - 1700nm) images for an (first column) SLR objective, (second column) proposed computational mirrors, and (third column) a plano-convex lens, all at 100mm focal length. The scene consisted of a printed USAF test target illuminated by broadband light. SLR objectives enable very sharp images in visible wavelengths (where they are optimized for), but are bulky and produce blur over broadband wavelengths. Plano-convex lenses enable better off-axis performance but even their visible performance is considerably poor. This primarily arises due to high variance in point spread function across the various wavelengths, as shown in the fourth column. Our computational mirrors are enabled by very light optics, and produce a sharp image across all wavelengths and full FoV.

loss of important details. All these results were captured with the same focus setting (v_0), implying there was no wavelength-dependent refocusing.

Comparison against glass-based objectives. To show the advantages of mirror-based optics for broadband VIS-SWIR imaging, Fig. 8 compares it against a mirrorless SLR 100mm zoom lens, and a plano-convex F/2 lens. Images captured by mirror optic were reconstructed with SeidelConv. We observe that Nikon lens produces sharpest image within the visible wavelengths, but has a blur when imaged over the full VIS-SWIR Wavelengths. Plano-convex in contrast has blurry image across any wavelength range owing to its severe chromatic aberration. In contrast, our mirror based optic produces sharp images independent of range. Additionally, our mirror-based optic weighs only 60g and has a 50mm length, whereas a 100mm Nikon lens weights more than 400g and is thrice as long.

Number of images in the focal stack. Fig. 9 shows deconvolution on our 50mm mirror objective for varying number of images in the focal stack. We notice that the quality improves with increasing number of images, but saturates after 3 images, motivating most of the experiments in this paper. It is worth noting that the number of images depends on the field curvature. For the same sensor size, a 25mm objective will have twice the curvature of a 50mm objective, likely necessitating more images in the focal stack. On the other hand, a 100mm objective has lower curvature, implying even two images may suffice. For longer focal lengths, we anticipate that even a single image can result in sharp images.

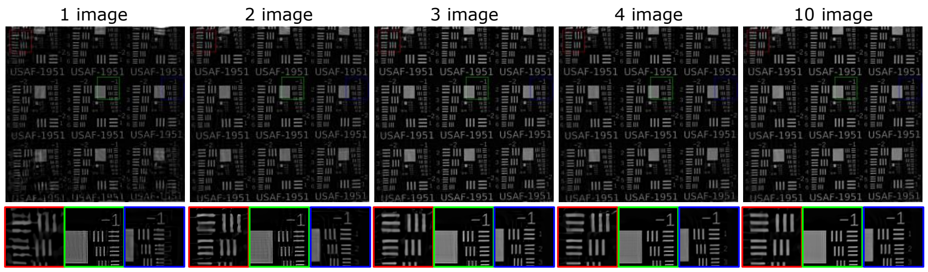

Fig. 9: Effect of number of images in focal stack. We show results for varying number of images in the focal stack for a 50mm, F/1 optic. As few as three images results in a dramatic improvement in off-axis resolution, compared to a single image. Additionally, performance plateaus after 3 images, making three a heuristically optimal number of images in this scenario.

5 Discussions and Conclusion

This work validates Computational Mirrors as a robust framework for high-aperture, ultra-broadband imaging. Using $f/1$ 50mm and $f/2$ 100mm prototypes, we demonstrated that a sparse focal stack of only three images is sufficient to reconstruct high-fidelity, all-in-focus imagery across the full field of view. The core of this capability is SeidelConv, a physically motivated and computationally efficient PSF model that, when paired with a PnP framework, effectively mitigates the severe geometric aberrations of simple reflective optics. Our results across the VIS, NIR, and SWIR spectra highlight the primary advantage of this approach: because reflective optics are inherently achromatic, they require no wavelength-dependent refocusing or PSF recalibration. With VIS-SWIR sensors, our method facilitates material characterization and identification in a compact form factor that was previously unattainable with refractive designs.

Limitations. Our approach requires multiple measurements to recover each image, implying that dynamic scenes may suffer from motion artifacts. However, recent advances in inter-measurement optical flow [35] enable robust realignment of images, and hence our approach can result in high quality full field of view images. While iterative solvers using Plug-and-Play (PnP) priors facilitate training-free reconstruction, their high computational cost can limit real-time deployment. A promising future direction is the development of end-to-end feed-forward networks that map focal stacks directly to sharp, all-in-focus images [36]. In this context, SeidelConv serves as a high-fidelity, differentiable forward model, enabling the generation of massive synthetic datasets to train these networks without the need for exhaustive physical data collection.

6 Acknowledgement

This work is supported in part by DTRA grant HDTRA12610007, CNS-2312395, CMMI-2326309, and a University of California Regents Faculty Fellowship.

References

1. José M Bioucas-Dias, Antonio Plaza, Gustavo Camps-Valls, Paul Scheunders, Nasser Nasrabadi, and Jocelyn Chanussot. Hyperspectral remote sensing data analysis and future challenges. *IEEE Geoscience and Remote Sensing Magazine*, 1(2):6–36, 2013. 1
2. Mercedes Eugenia Paoletti, Juan Mario Haut, Javier Plaza, and Antonio Plaza. Deep learning classifiers for hyperspectral imaging: A review. *J. Photogrammetry and Remote Sensing*, 158:279–317, 2019. 1
3. Anuja Bhargava, Ashish Sachdeva, Kulbhushan Sharma, Mohammed H Alsharif, Peerapong Uthansakul, and Monthippa Uthansakul. Hyperspectral imaging and its applications: A review. *Heliyon*, 10(12), 2024. 1
4. Lang Junwei, Wang Yueming, Xiao Xizhong, Zhuang Xiaoqiong, Wang Shengwei, Liu Jun, and Wang Jianyu. Study on shortwave infrared long-distance imaging performance based on multiband imaging experiments. *Optical Engineering*, 52(4):045008–045008, 2013. 1
5. Jürgen Krieg and Uwe Adomeit. Comparative long-time visible and shortwave infrared night illumination measurements. *Appl. Optics*, 58(36):9876–9882, 2019. 1
6. Dietrich Korsch. *Reflective Optics*. Academic Press, 2012. 2
7. KP Norris, WE Seeds, and MHF Wilkins. Reflecting microscopes with spherical mirrors. *J. Optical Society of America*, 41(2):111–119, 1951. 2, 4
8. Jonathan P Gardner, John C Mather, Randy Abbott, James S Abell, Mark Abernathy, Faith E Abney, John G Abraham, Roberto Abraham, Yasin M Abul-Huda, Scott Acton, et al. The James Webb Space Telescope Mission. *Astronomical Society of the Pacific*, 135(1048):068001, 2023. 2
9. Rudolf Kingslake and R Barry Johnson. *Lens design fundamentals*. Academic Press, 2009. 2
10. Max Jaderberg, Karen Simonyan, Andrew Zisserman, et al. Spatial transformer networks. *Adv. Neural Info. Processing Systems*, 28, 2015. 3
11. Esther YH Lin, Zhecheng Wang, Rebecca Lin, Daniel Miau, Florian Kainz, Jiawen Chen, Xuaner Zhang, David B Lindell, and Kiriakos N Kutulakos. Learning lens blur fields. *IEEE Trans. Pattern Analysis and Machine Intelligence*, 47(9):7383–7395, 2025. 3, 8
12. Kai Zhang, Yawei Li, Wangmeng Zuo, Lei Zhang, Luc Van Gool, and Radu Timofte. Plug-and-play image restoration with deep denoiser prior. *IEEE Trans. Pattern Analysis and Machine Intelligence*, 44(10):6360–6376, 2021. 3, 9, 11
13. Max Born and Emil Wolf. *Principles of Optics: Electromagnetic Theory of Propagation, Interference and Diffraction of Light*. Cambridge University Press, 7th edition, 1999. 4, 7
14. Dietrich Korsch. Anastigmatic three-mirror telescope. *Appl. Optics*, 16(8):2074–2077, 1977. 4
15. E Tseng, S Colburn, J Whitehead, L Huang, SH Baek, A Majumdar, and F Heide. Neural nano-optics for high-quality thin lens imaging nat. *Nature Communications*, 12:1–7, 2021. 4
16. Johannes E Fröch, Praneeth Chakravarthula, Jipeng Sun, Ethan Tseng, Shane Colburn, Alan Zhan, Forrest Miller, Anna Wirth-Singh, Quentin AA Tanguy, Zheyi Han, et al. Beating spectral bandwidth limits for large aperture broadband nano-optics. *Nature Communications*, 16(1):3025, 2025. 4

17. Shi Mao, Yogeshwar Mishra, and Wolfgang Heidrich. Fovea stacking: Imaging with dynamic localized aberration correction. *ACM Trans. Graphics*, 44(6), 2025. 4
18. Viktoria V Evdokimova, Vladimir V Podlipnov, Nikolay A Ivliev, Maxim V Petrov, Sofia V Ganchevskaya, Vladimir A Fursov, Yuriy Yuzifovich, Sergey O Stepanenko, Nikolay L Kazanskiy, Artem V Nikonorov, et al. Hybrid refractive-diffractive lens with reduced chromatic and geometric aberrations and learned image reconstruction. *Sensors*, 23(1):415, 2022. 4
19. SeyyedReza MiriRostami, Samuel Pinilla, Igor Shevkunov, Vladimir Katkovnik, and Karen Egiazarian. Hybrid diffractive optics (doe & refractive lens) for broadband edof imaging. *Electronic Imaging*, 35:1–14, 2023. 4
20. Tie Hu, Shengqi Wang, Yunxuan Wei, Liqinng Wen, Xing Feng, Zhenyu Yang, Jinkun Zheng, and Ming Zhao. Design of a centimeter-scale achromatic hybrid metalens with polarization insensitivity in the visible. *Optics Letters*, 48(7):1898–1901, 2023. 4
21. Mehdi Bahrami and Alexander V Goncharov. All-spherical catadioptric telescope design for wide-field imaging. *Appl. Optics*, 49(30):5705–5712, 2010. 4
22. John J Villa. Adaptation of the schupmann medial telescope to a large scale astronomical optical system. *Appl. Optics*, 11(8):1814–1821, 1972. 4
23. Ryunosuke Yokoya and Shree K Nayar. Extended depth of field catadioptric imaging using focal sweep. In *IEEE Comp. Vision and Pattern Recognition (CVPR)*, 2015. 5, 11, 12
24. Shigehiko Matsunaga and Shree K Nayar. Field curvature correction using focal sweep. *IEEE Trans. Computational Imaging*, 1(4):259–269, 2015. 5, 7, 11, 12
25. Sara Abrahamsson, Jiji Chen, Bassam Hajj, Sjoerd Stallinga, Alexander Y Katsov, Jan Wisniewski, Gaku Mizuguchi, Pierre Soule, Florian Mueller, Claire Dugast Darzacq, et al. Fast multicolor 3D imaging using aberration-corrected multifocus microscopy. *Nature Methods*, 10(1):60–63, 2013. 5
26. Eric Kee, Sylvain Paris, Simon Chen, and Jue Wang. Modeling and removing spatially-varying optical blur. In *IEEE Intl. Conf. Computational Photography (ICCP)*. IEEE, 2011. 7
27. Joel Yeo, N Duane Loh, Ramon Paniagua-Dominguez, and Arseniy I Kuznetsov. EigenCWD: A spatially varying deconvolution algorithm for single metalens imaging. *Optics Express*, 33(13):28481–28492, 2025. 7, 8
28. Sarah Frisken Gibson and Frederick Lanni. Experimental test of an analytical model of aberration in an oil-immersion objective lens used in three-dimensional light microscopy. *J. Optical Society of America A*, 8(10):1601–1613, 1991. 7
29. Amit Kohli, Anastasios N Angelopoulos, David McAllister, Esther Whang, Sixian You, Kyrollos Yanny, Federico M Gasparoli, Bo-Jui Chang, Reto Fiolka, and Laura Waller. Ring deconvolution microscopy: exploiting symmetry for efficient spatially varying aberration correction. *Nature Methods*, 22(6):1311–1320, 2025. 7, 11, 12
30. Jin Gong, Runzhao Yang, Weihang Zhang, Jinli Suo, and Qionghai Dai. A physics-informed low-rank deep neural network for blind and universal lens aberration correction. In *IEEE Comp. Vision and Pattern Recognition (CVPR)*, 2024. 7
31. Nicholas Chimitt and Stanley H Chan. Simulating anisoplanatic turbulence by sampling intermodal and spatially correlated zernike coefficients. *Optical Engineering*, 59(8):083101–083101, 2020. 7
32. Sunny Howard, Peter Norreys, and Andreas Döpp. CoordGate: Efficiently computing spatially-varying convolutions in convolutional neural networks. In *British Machine Vision Conference*, 2024. 8, 12

33. Felix Heide, Mushfiqur Rouf, Matthias B. Hullin, Bjorn Labitzke, Wolfgang Heidrich, and Andreas Kolb. High-quality computational imaging through simple lenses. *ACM Trans. Graphics*, 32(5), 2013. 11, 12
34. Kodak lossless true color image suite. `http://r0k.us/graphics/kodak/`, 1999. Accessed: 2026-06-30. 11
35. Yihan Wang, Lahav Lipson, and Jia Deng. Sea-raft: Simple, efficient, accurate raft for optical flow. In *IEEE European Conf. Computer Vision (ECCV)*, 2024. 15
36. Xiu Li, Jinli Suo, Weihang Zhang, Xin Yuan, and Qionghai Dai. Universal and flexible optical aberration correction using deep-prior based deconvolution. In *IEEE Comp. Vision and Pattern Recognition (CVPR)*, 2021. 15